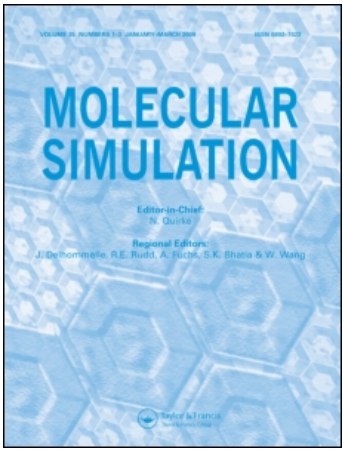

Molecular Simulation

Publication details, including instructions for authors and subscription information:
http://www.informaworld.com/smpp/title~content=t713644482

Computer Modelling and Exafs Study of the Disorder In $Cd_{1-x}Pb_xF_2$ Mixed Systems

T. T. Netshisaulu[a]; P. E. Ngoepe[ab]; A. V. Chadwick[c]

[a] Materials Modelling Centre, University of the North, Sovenga, South Africa [b] Division of Materials Science and Technology, CSIR, Pretoria, South Africa [c] Department of Chemistry, University of Kent, Canterbury, UK

To cite this Article Netshisaulu, T. T. , Ngoepe, P. E. and Chadwick, A. V.(1999) 'Computer Modelling and Exafs Study of the Disorder In $Cd_{1-x}Pb_xF_2$ Mixed Systems', Molecular Simulation, 22: 1, 1 — 21
To link to this Article: DOI: 10.1080/08927029908022082
URL: http://dx.doi.org/10.1080/08927029908022082

Molecular Simulation, 1999, Vol. 22, pp. 1–21
Reprints available directly from the publisher
Photocopying permitted by license only

COMPUTER MODELLING AND EXAFS STUDY OF THE DISORDER IN $Cd_{1-x}Pb_xF_2$ MIXED SYSTEMS

T. T. NETSHISAULU[a], P. E. NGOEPE[a,c] and A. V. CHADWICK[b,*]

[a] *Materials Modelling Centre, University of the North, P/Bag X1106, Sovenga, 0727, South Africa;*
[b] *Department of Chemistry, University of Kent, Canterbury, CT2 7NH, UK;*
[c] *Division of Materials Science and Technology, CSIR, Pretoria 0001, South Africa*

(Received October 1998; accepted November 1998)

We report molecular dynamics and EXFAFS studies of $Cd_{0.4}Pb_{0.6}F_2$ mixed system. A striking feature of molecular dynamics studies in $Cd_{0.4}Pb_{0.6}F_2$ is the mobility of F^- ions below. T_c calculations of defect activation energies and plots of single ion trajectories in this compound show that fluorine ions migrate predominantly by a near interstitialcy mode of migration. The results obtained from EXAFS studies on local environments around Cd and Pb cations in this system are consistent with the findings from computer simulations on radial distribution functions. The local environment of Pb^{2+} ions is more disordered than that of Cd^{2+} ions.

Keywords: Molecular dynamics; EXAFS; $Cd_{0.4}Pb_{0.6}F_2$; mean square displacement; radial distribution functions

1. INTRODUCTION

Mixed crystals, $Cd_{1-x}Pb_xF_2$, form a continuous series of substitutional solid solutions with the fluorite structure [10–14]. The anomalies in ionic conductivities and elastic constants of fast-ion conductors (both pure crystalline and those containing defects) are associated with the development of extensive disorder on the anion sublattice.

Divalent doping of fluorites, modifies their transport properties quite significantly. Recent high temperature studies of $Cd_{1-x}Pb_xF_2$ using techniques

*Corresponding author.

such as Raman scattering [10–14] have provided strong evidence for enhanced fluorine anion (F^-) diffusion, particularly below the transition temperature (T_c) to the fast-ion phase.

Previous EXAFS studies on mixed-metal fluorides with very high F^- ion conductivities, such as $RbBiF_4$ and $PbSnF_4$, successfully revealed the local structural environments of their respective cations [5, 7, 8]. The main features of note were the contrasts between the temperature dependence of the cation – anion amplitudes and frequencies. Furthermore, F^- vacancies were preferentially located on anion sites neighbouring cations having larger ionic radii and lower charges. This intriguing behaviour was attributed to the fact that it is easier to remove ions from sites close to singly charged ions (*e.g.*, Rb in $RbBiF_4$) than from sites adjacent to the more highly charged Bi ions. However, in $Cd_{0.4}Pb_{0.6}F_2$, both cations have the same charge (+2) as in $PbSnF_4$ [7], so that no electrostatic advantage exists for the creation of F^- vacancies in anion sites adjacent to the cations.

A detailed understanding of structural properties, elastic constants, defect energetics and transport mechanisms occurring in CdF_2–PbF_2 compounds remain elusive. For these reasons it is necessary to carry out a predictive theoretical and EXAFS experimental studies (which have been applied with considerable success in studying analogous features in more complex materials) on $Cd_{1-x}Pb_xF_2$ systems.

In the present study, computer modelling and EXAFS techniques are used to elucidate the temperature dependence of the local structural features, surrounding both the host Cd^{2+} and dopant Pb^{2+} cations, within CdF_2–PbF_2 systems. In this study, structural properties, particularly the local environment of the cations and conduction mechanisms in $Cd_{0.4}Pb_{0.6}F_2$ are investigated in an effort to better understand the physics and chemistry of this intriguing fast-ion conductor. $Cd_{0.4}Pb_{0.6}F_2$ compound has been particularly chosen since it exhibits the lowest T_c across the $Cd_{1-x}Pb_xF_2$ composition range [14].

2. COMPUTATIONAL PROCEDURE

The lattice potentials of $Cd_{0.4}Pb_{0.6}F_2$ were taken from those of the appropriate binary fluorides. Hence, empirically derived interionic potentials of CdF_2 were employed, and the shell model parameters used for PbF_2 were those of Jacobs *et al.* [9]. The details of the parameters so determined for $Cd_{0.4}Pb_{0.6}F_2$ are given in Table I.

Appropriate physical properties of $Cd_{0.4}Pb_{0.6}F_2$ such as dielectric and elastic constants were calculated by means of the THBREL code as outlined

TABLE I Potential parameters of $Cd_{0.4}Pb_{0.6}F_2$

Shell model parameters

Ion	$Y(\|e\|)$	$K(eV\mathring{A}^{-2})$
Cd^{2+}	−4.315	741.4
Pb^{2+}	−4.39	192.935
F^-	−1.96	101.2

Short-range parameters

Ion *Interaction*	A_{ij} (eV)	ρ_{ij} $(\mathring{A})$	C_{ij} $(eV\mathring{A}^{-6})$
$Cd^{2+} - Cd^{2+}$	0.00	0.00	0.00
$Cd^{2+} - F^-$	2485.9	0.2672	0.00
$Pb^{2+} - Pb^{2+}$	0.00	0.00	0.00
$Pb^{2+} - F^-$	381.9	0.4115	0.00
$Cd^{2+} - Pb^{2+}$	0.00	0.00	0.00
F − F	1127.72	0.2753	0.00

in Netshisaulu *et al.* [16]. The temperature variation of the lattice parameter as determined by Kosacki *et al.* [14] is presented in Figure 1.

In order to obtain accurate values of defect energies, the ions surrounding the defect were relaxed using sell model potentials. As outlined in Netshisaulu *et al.* (1993), a normal fluorite structure was used as a starting point. Secondly, ions were introduced into/removed from the lattice from/to infinity. Calculations on defect energies were conducted on several configurations (not shown here). The present calculations are based on the configurations which yield minimum energy of point defects (Figs. 2a−d) and a reliable value of the anion Frenkel formation energy of $Cd_{0.4}Pb_{0.6}F_2$. As shown in Figure 2a, for the determination of the anion vacancy formation energy, the anion vacancy was surrounded by four cation nearest neighbours (two Cd^{2+} forming a top layer and two Pb^{2+} cations forming the bottom layer) at tetrahedral positions.

Calculations of migration energy assume that it is sufficient to locate the lowest saddle point on the migration path. These calculations were performed in stages. In the present investigation, the saddle point for vacancy migration was located with the moving ion placed mid-way between two anion lattice sites (see Fig. 2c). The appropriate activation energy was determined from the difference between the energetics of defect formation and migration.

A similar approach was followed for the determination of both interstitial formation and migration energies (Figs. 2b and 2d). A configuration for the displacive interstitialcy migration mechanism was employed for the present calculations on anion interstitial migration energies. Furthermore, Figure 2d depicts that ionic migration processes shown are determined by

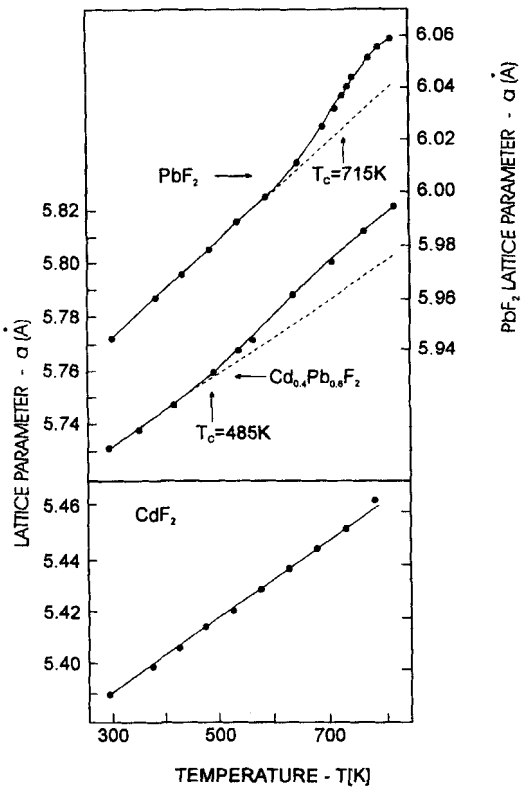

FIGURE 1 The temperature dependence of lattice parameter for $Cd_{0-4}Pb_{0-6}F_2$ crystals. (After Kosacki *et al.*, 1989).

the movement of those fluorine ions whose nearest-neighbourhood contains the Pb ions.

The Fungus code was used for MD calculations which yields valuable information on the defect structure and transport properties of ionic crystals [4]. As in previous MD simulations of similar fast-ion conductors [6], empirically derived rigid-ion potentials were employed, with coordinates and velocities updated using suitable algorithm (*e.g.*, Beeman's algorithm). A time-step of 5 fs was used. In the fluorite structure of $Cd_{1-x}Pb_xF_2$, the two cation species, *i.e.*, Cd and Pb, form a face-centred cubic lattice. First Cd ions were placed on all alternate cube center sites, forming CdF_2. Next a suitable number of Cd ions were replaced at random by Pb ions forming $Cd_{0.4}Pb_{0.6}F_2$.

Since we wish to compare our results with those of experiments at certain temperatures, it is instructive to conduct several dynamical simulation runs

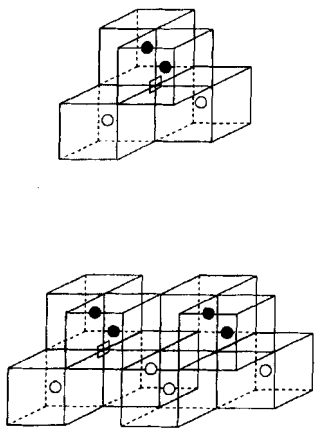

FIGURE 2a Vacancy formation.

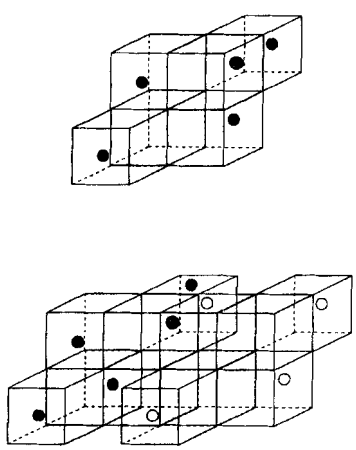

FIGURE 2b Interstitial formation.

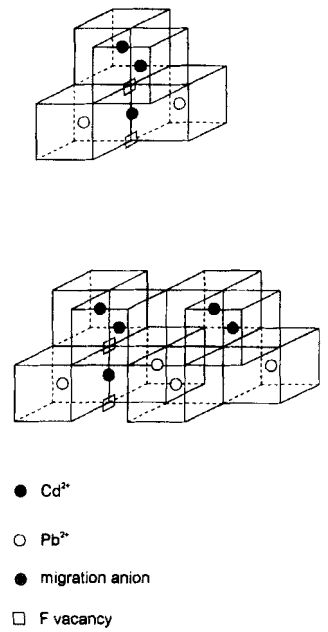

FIGURE 2c Vacancy migration.

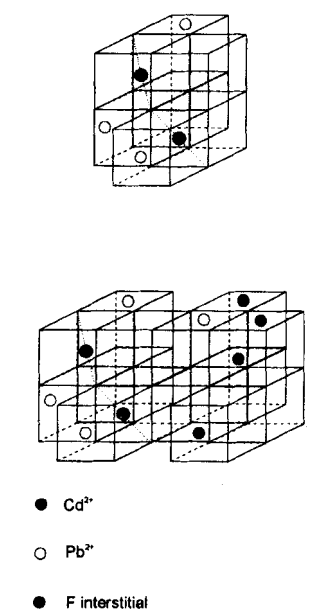

FIGURE 2d Interstitial migration energy.

at temperatures corresponding to those used in EXAFS measurements. Time dependent structural properties were extracted from MD studies *via* the radial distribution functions (RDFs), and were compared with EXAFS results.

3. EXPERIMENTAL DETAILS

3.1. Sample Preparations

The 2:3 mixtures of CdF_2 and β-PbF_2 powders of high purity (> 99.99%) were intimately mixed and melted in quartz tubes at temperatures above 1100 K until a uniformly clear melt was obtained under high vacuum (10^{-6} torr). The preparations were carried out in the Chemical Laboratory of the University of Kent, in Canterbury, UK. Crystalline PbF_2 was prepared as a reference specimen in EXAFS analysis for the Pb edge in $Cd_{0.4}Pb_{0.6}F_2$, whilst powdered CdF_2 was used for the Cd edge. X-ray diffraction patterns were collected to check that single cubic fluorite phase crystals had been prepared. The prepared specimens were finely ground (< 20 μm) with a mortar and presstle and well diluted with silica and boron nitride into thin coherent pellets (200–400 μm) using a 13 mm die. Suitable thicknesses were obtained by trial and error.

3.2. EXAFS Data Collection

The EXAFS measurements of $Pb(L_{111})$ (above 13.036 keV) and Cd(K) (above 26.716 keV) edges in $Cd_{0.4}Pb_{0.6}F_2$ were carried out using the Science and Engineering Council (SERC) synchrotron radiation facilities at the Daresbury Laboratory in Great Britain. Data acquisition were carried out on EXAFS stations 7.1 [for the $Pb(L_{111})$ edge] and 9.2 [for the Cd(K) edge]. The samples were mounted in an evacuable crystal heating furnace with Beryllium windows. X-ray absorption spectra for the two edges were then measured at various temperatures in the transmission mode using a channel-cut silicon (111) crystal monochromator to study the $Pb(L_{111})$ absorption edge and the silicon (220) one for the Cd(K) edge. Monochromators were used to minimise harmonic contamination of the beam. The incident (I_o) and the transmitted (I_t) intensities of the X-ray beam were measured by the (75% N_2 + 25% Ar) and the 100% Kr ion chambers, respectively. All scans were typically 40 min. duration. During the data collection, the SRS operated at an energy of about 2.0 GeV with a typical beam current of 150 mA.

3.3. Data Analysis

The EXAFS spectra were averaged and calibrated using the EXCALIB program and background subtraction was accomplished with EXBACK program. The subsequent data was analyzed using an iterative EXCURV92 program which generates theoretical spectra. The program also enabled us to effect the Fourier transformation of spectra frequency to distance space. The phase shifts for a particular atom pair were obtained empirically, and refined using appropriate model compounds with known geometries (in this work CdF_2 and PbF_2 were used), taking the crystallographically determined distances as starting points.

4. RESULTS

4.1. Computational

4.1.1. Molecular Statics Calculations

Although rigid-ion potentials are good enough for computational studies, in calculations which are to be compared with experiments, it is most preferable to use good shell model interionic potentials. Consequently, Table II summarises the crystal bulk data of $Cd_{0.4}Pb_{0.6}F_2$ calculated on the basis of the shell model potentials (see Tab. I). Interionic potentials have been found to be adequate in molecular dynamics simulations provided that static dielectric constants are correctly predicted [2]. Hence, in the absence of firm data for comparison, the present investigation on elastic properties have been based on a known static dielectric constant of ≈ 15 deduced from conductivity measurements conducted by Kosacki *et al.* [10, 13] on the material. It is interesting to note that the calculated value of the dielectric constant compares remarkably well with the experimental value (see Tab. II).

There exists order–disorder phase transition in the lattice parameter for $Cd_{0.4}Pb_{0.6}F_2$ [14]. This phase transition displays itself in the rapid increase of the lattice constant (Fig. 1). For temperatures above 620 K, the lattice constant of PbF_2 increases rather rapidly. Analogous anomalies at temperatures lower than for PbF_2, *i.e.*, at $T \simeq 485$ K, are observed for $Cd_{0.4}Pb_{0.6}F_2$ crystal. Examination of the lattice constant profile for CdF_2 reflects a complete absence of any pronounced anomaly in the anion sublattice for $T < 800$ K.

Table III presents various calculated defect energies of $Cd_{0.4}Pb_{0.6}F_2$. Owing to the present lack of most experimental quantities for this material, the

TABLE II Properties of perfect lattice

Property	*Calculated* $Cd_{0.4}Pb_{0.6}F_2$	*Calculated* CdF_2	*Calculated* PbF_2
Elastic constants (GPa)			
C_{11}	123.1	188.1	107.7
C_{12}	27.61	48.1	42.6
C_{44}	20.12	19.6	28.4
Dielectric constants			
ϵ_0	16.07 (15)*	9.96	17.6
ϵ_{00}	1.615	2.23	1.87

* Experimental value after Kosacki *et al.* (1989).

TABLE III Shell model defect formation and migration energies of $Cd_{0.4}Pb_{0.6}F_2$

Defect type	$Cd_{0.4}Pb_{0.6}F_2$ *Calc.* (*eV*)	*Exp.* (*eV*)	CdF_2 (*eV*)	PbF_2 (*eV*)
Anion vacancy	2.741		4.467	3.312
Anion interstitial	−2.137		−2.103	−2.017
Anion Frenkel pair	0.604	(0.6)	2.75	1.295
Anion vacancy migration	2.643		4.764	
Anion interstitial migration	−3.388		−1.358	
Anion vacancy activation*	−0.120		0.297	0.235
Anion interstitial-activation	−1.423		0.745	0.476
Anion vacancy activation†	0.564	(0.533)		

* Energy for the low temperature fluorine ion conduction.
† Energy for the high temperature fluorine ion conduction.

computed values are compared with those calculated for the corresponding pure fluorides (*i.e.*, CdF_2 and PbF_2). A direct comparison of our calculated anion Frenkel formation energy with the experimental value shows a satisfactory agreement. However, a comparison of the anion Frenkel energy obtained for $Cd_{0.4}Pb_{0.6}F_2$ with those of the two binary fluorides, *i.e.*, PbF_2 and CdF_2, reveals a considerable difference. Furthermore, the calculated formation energies for isolated vacancies and interstitials which led to a significantly low Frenkel energy are lower than those of both CdF_2 and PbF_2.

Defect activation energies which offer useful insights into the nature of the disorder are also reported in Table III. The computer simulated value for the activation energy (E_{act}) determined for high temperature conduction, which shows the fluorine ion contribution to the transport, is equal to 0.564 eV. This value is in excellent accord with that obtained by Kosacki *et al.* [14] for $Cd_{0.4}Pb_{0.6}F_2$ as indicated in Table III. The fluorine ion activation energy which is connected with a motion of the fluorine vacancies introduced in the crystal is presently determined for the first time. The value of this

energy is very low ($\simeq -0.1$ eV) compared to that of CdF_2 ($\simeq 0.3$ eV), but higher than the anion interstitial activation energy ($E_{act} \simeq -1.4$ eV).

4.1.2. MD Calculations

Figure 3a shows five typical mean-square displacement (MSD) graphs for $Cd_{0.4}Pb_{0.6}F_2$ at temperatures 100, 400, 500, 600 and 800 K. It can be observed that, diffusion for fluorine species, increases with an increase in temperature. This is reflected with the diffusion constant *vs.* temperature profile presented in Figure 4. However, it is clear that the Cd and Pb ions do not diffuse at all investigated temperatures, *i.e.*, they maintain the fluorite structure (see Fig. 3b). Figure 5 presents the variation of the MSD of the fluorine ion species with time in parent compounds, CdF_2 and PbF_2, and in $Cd_{0.4}Pb_{0.6}F_2$ compound at 400 K. It is noted that F^- motion occurs only in $Cd_{0.4}Pb_{0.6}F_2$.

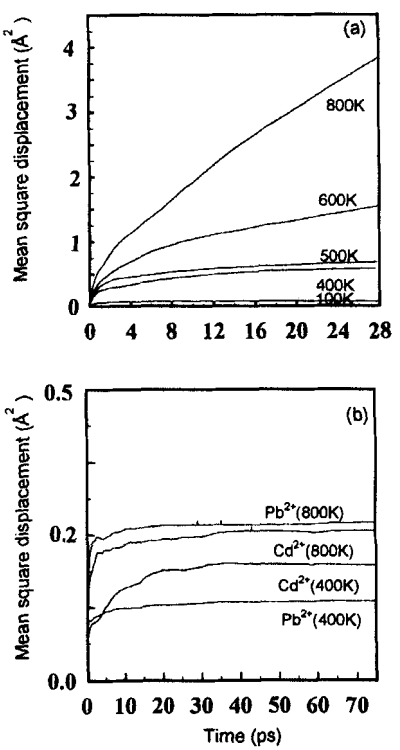

FIGURE 3 Mean square displacements of (a) F^- ions and (b) Cd^{2+} and Pb^{2+} ions in $Cd_{0-4}Pb_{0-6}F_2$ at various temperatures.

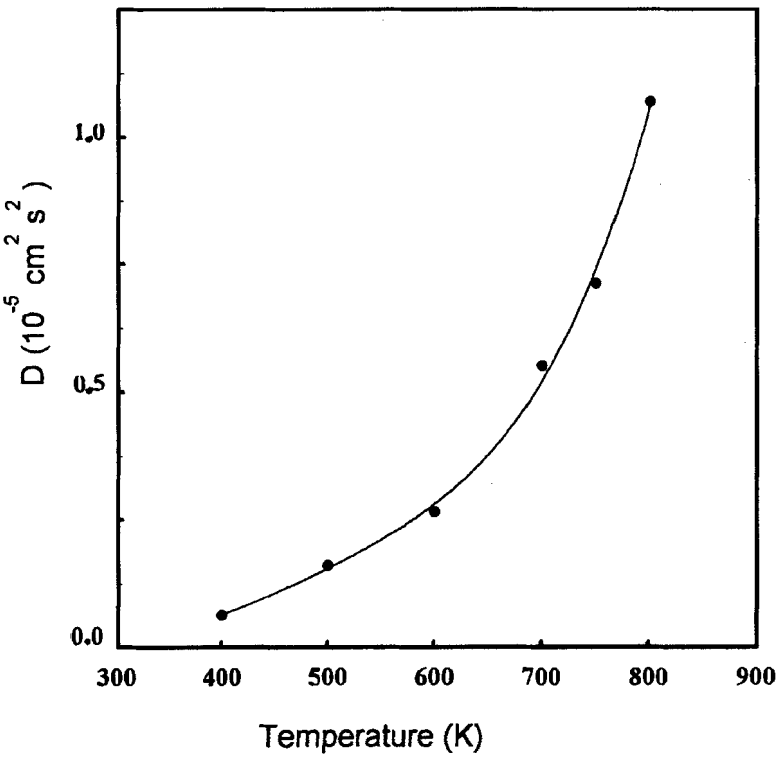

FIGURE 4 Anion diffusion coefficient calculated from the present simulations on $Cd_{0-4}Pb_{0-6}F_2$.

Transport of F^- ions occurs *via* diffusion between interstitial sites. A typical example is shown in Figure 6, where a F^- ion oscillates around an interstitial position then move and occupy a regular lattice site, before moving out again into an interstitial position.

In order to obtain more definite information on local structures in $Cd_{0.4}Pb_{0.6}F_2$, the radial distribution functions (RDFs) for all pairs of ions were calculated. Cd–F and Pb–F RDFs at 300 and 500 K are shown in Figure 7. Features of interest, *i.e.*, the Cd–F and Pb–F nearest neighbour (NN) distances or the positions of the first peaks of the RDFs were depicted from Figure 7 and reported in Tables VI, VII and VIII.

4.2. Experimental

The radial distribution functions were obtained by Fourier transforming the EXAFS function [χ(k)] data. The Fourier transforms [experimental (——)

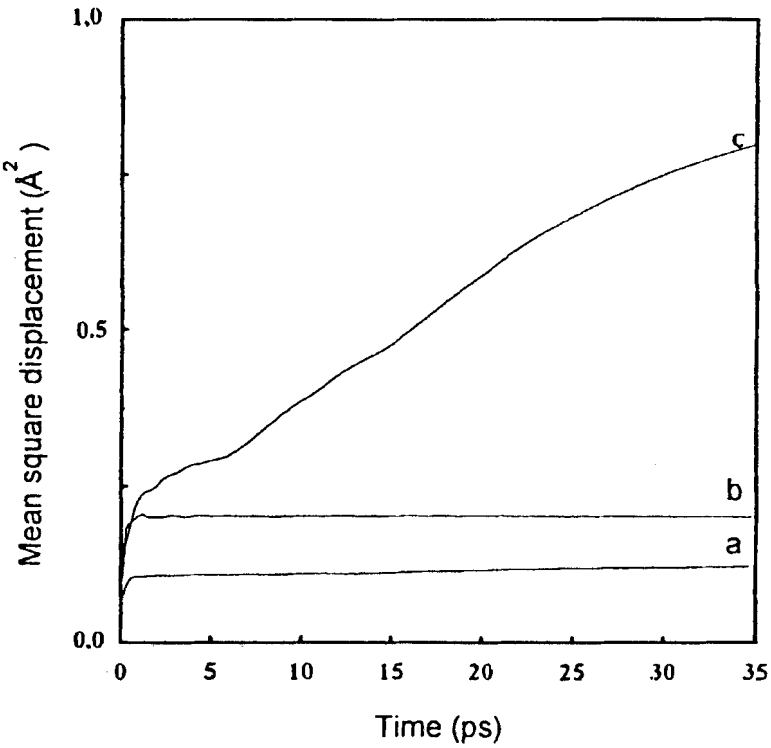

FIGURE 5 Mean square displacements of F^- ions in (a) CdF_2 (b) PbF_2 (c) $Cd_{0-4}Pb_{0-6}F_2$ at 400 K.

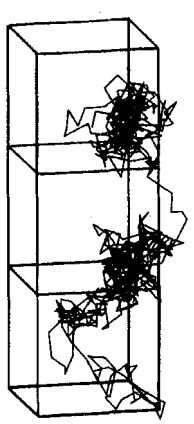

FIGURE 6 Ion migration mechanism for the F^- ion in $Cd_{0-4}Pb_{0-6}F_2$ at 800 K.

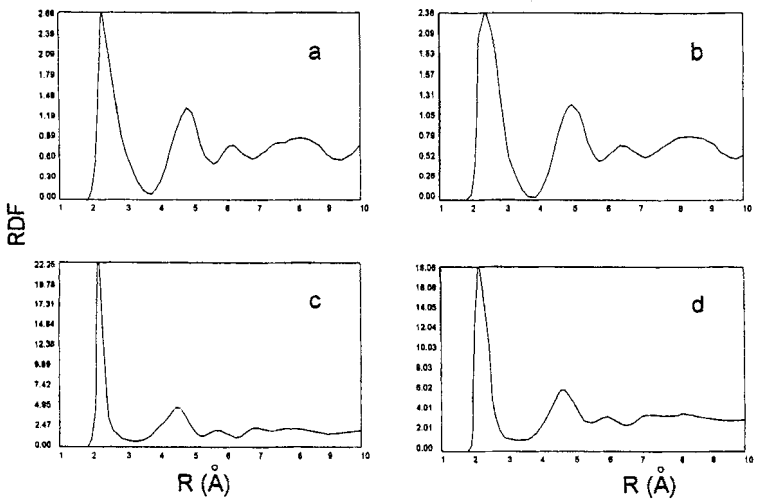

FIGURE 7 Pb–F [(a) and (b)] and Cd–F [(c) and (d)] radial distribution functions for the $Cd_{0-4}Pb_{0-6}F_2$ at 300 and 500 K, respectively.

TABLE IV A comparison of the values for the EXAFS and simulated radial distances (RD), Debye-Waller factors and coordination numbers (N) for the Cd edge in CdF_2 as a function of temperature

T(K)	*Atom type*	*Coordination number N*	*Simulated RD (Å)*	*EXAFS RD (Å)*	*Debye-Waller factor ($Å^2$)*
300	F	8	2.269	2.275	0.015
	Cd	12	3.808	3.814	0.014
500	F	8	2.308	2.297	0.032
	Cd	12	3.798	3.861	0.034

TABLE V A comparison of the values for the EXAFS and simulated radial distances (RD), Debye-Waller factors and coordination numbers (N) for the Pd edge in PbF_2 as a function of temperature

T(K)	*Atom type*	*Coordination number N*	*Simulated RD (Å)*	*EXAFS RD (Å)*	*Debye-Waller factor ($Å^2$)*
300	F	8	2.458	2.491	0.045
	Pb	12	4.192	4.217	0.027
450	F	8	2.408	2.448	0.059
	Pb	12	4.192	4.211	0.043
500	F	8	2.388	2.427	0.064
	Pb	12	4.212	4.203	0.044

and theoretical EXAFS (– – – –)] of the Cd(K) and Pb(L_{111}) edges are reported in Figure 8 for the CdF_2 and for the PbF_2 reference compounds, respectively. RDFs around Cd^{2+} and Pb^{2+} cations were obtained *via* a

TABLE VI Comparison of the values for the EXAFS and simulated radial distances (RD), Debye-Waller factors and coordination numbers (N) for the Cd edge in $Cd_{0.4}Pb_{0.6}F_2$ as a function of temperature

T(K)	*Atom type*	*Coordination number N*	*Simulated RD (Å)*	*EXAFS RD (Å)*	*Debye-Waller factor ($Å^2$)*
300	F	8	2.192	2.227	0.024
	Cd	12	3.735	3.887	0.050
450	F	8	2.192	2.220	0.031
	Cd	12	3.735	3.899	0.063
500	F	8	2.190	2.219	0.033
	Cd	12	3.769	3.924	0.063

TABLE VII Comparison of the values for the EXAFS and simulated radial distances (RD), Debye-Waller factors and coordination numbers (N) for the Pb edge in $Cd_{0.4}Pb_{0.6}F_2$ as a function of temperature

T(K)	*Atom type*	*Coordination number N*	*Simulated RD (Å)*	*EXAFS RD (Å)*	*Debye-Waller factor ($Å^2$)*
300	F	8	2.539	2.471	0.053
	Pb	12	4.177	4.192	0.050
450	F	8	2.500	2.453	0.065
	Pb	12	4.173	4.166	0.050
500	F	8	2.500	2.437	0.077
	Pb	12	4.173	4.131	0.057

TABLE VIII Computer simulations nearest neighbour distance for $Cd_{0.4}Pb_{0.6}F_2$ as a function of temperature

T(K)	*Cd – Pb*	*F – F*
300	4.039	3.210
450	4.039	3.192
500	4.039	3.230

Fourier transform of the k^3-weighted EXAFS function [$\chi(k)$] for the two edges as explained in the Introduction. Both profiles clearly reveal the presence of two peaks corresponding to cation–anion (first shell) and cation–cation (second shell) radial distances. The first peaks in the Fourier transforms of the Cd(K) and the Pb(L_{III}) edges in CdF_2 and PbF_2 result from the backscattering corresponding to the first shell cation–anion interactions (*i.e.*, Cd–F and Pb–F interatomic distances) while the second peaks correspond to the backscattering from the second shell cation–cation interactions (*i.e.*, Cd–Cd and Pb–Pb, respectively). The best fit values for radial distances, Debye-Waller factors and number of nearest-neighbours obtained from the EXAFS data are presented in Table IV for the Cd edge and in Table V for the Pb edge.

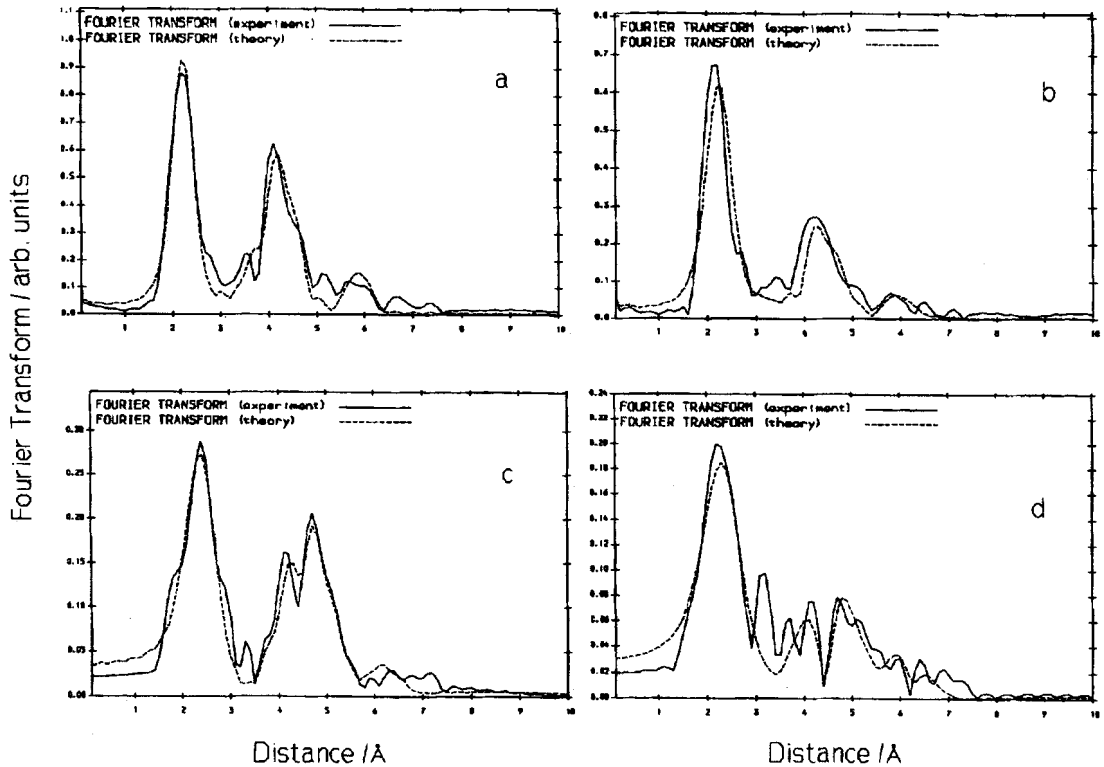

FIGURE 8 EXAFS experimental Fourier Transforms for the Cd [(a) and (b)] and Pb [(c) and (d)] edges in CdF_2 and PbF_2 at 300 and 500 K, respectively.

Figure 9 shows Fourier transform plots for the experimental and theoretical absorption spectra for the Pb and Cd edges in $Cd_{0.4}Pb_{0.6}F_2$ at temperatures 300 and 500 K, respectively. Although both RDFs consist of only one well-defined peak, their spectra are different, suggesting different local geometries for the two cations in $Cd_{0.4}Pb_{0.6}F_2$. In Tables VI and VII, we compare our EXAFS and simulation bond lengths. In each case, the dopant is surrounded by 8 fluorides as in the case of the host (Cd) ions, *i.e.*, in this study, coordination numbers were kept fixed to their preset values.

5. DISCUSSIONS

Our computer simulation studies have been used to predict bulk crystal data of $Cd_{0.4}Pb_{0.6}F_2$, which are currently scarce. An accurate reproduction of the experimental dielectric constant [14] depicts the reliability of calculations. A higher value of this quantity compared to that of CdF_2, indicates that doping promotes dipole polarization of thermally generated lattice defects in these crystals. Such high values are not observed in typical crystals and are specific for liquid electrolytes or fast-ion conductors (Kosacki, 1988).

The lowest-energy configuration were employed in defect energy calculations of $Cd_{0.4}Pb_{0.6}F_2$. A low value of the anion Frenkel pair formation energy (see Tab. III) in this compound could be attributed to its complex structure caused by the presence of the Pb ions in $Cd_{0.4}Pb_{0.6}F_2$ [11–14]. Such cations lead to an increase in the F^- ion disorder which is manifested in (a) a drop in the temperature to the fast-ion phase (T_c) (by about 220 K) (b) a significant reduction in the activation energy of conductivity and (c) an exceptionally high room-temperature fluorine ion conductivity of $Cd_{0.4}Pb_{0.6}F_2$.

Examination of the very low anion interstitial activation energy of ionic conduction presented in Table III suggests that near interstitialcy mechanism is a more prevalent mode of transport in $Cd_{0.4}Pb_{0.6}F_2$. Such an interstitialcy migration mechanism is also depicted from single ion trajectories obtained from our molecular dynamics calculations. This conclusion is further supported by Ngoepe and Catlow [18], where they propose that interstitialcy mechanism, rather than vacancy, is predominant in fluorites in the presence of aliovalent dopants. However, this is in contrast with the vacancy migration mechanisms reported for several pure fluorites [*e.g.*, CdF_2 and PbF_2 [17], CaF_2 [1, 18], $SrCl_2$ [1] and in $(ZrO_2)_{1-x}(Y_2O_3)_x$].

Molecular dynamics investigations on $Cd_{0.4}Pb_{0.6}F_2$ reveal that F^- ion diffusion occurs at significantly low temperatures ($< T_c \simeq 485$ K) and persists

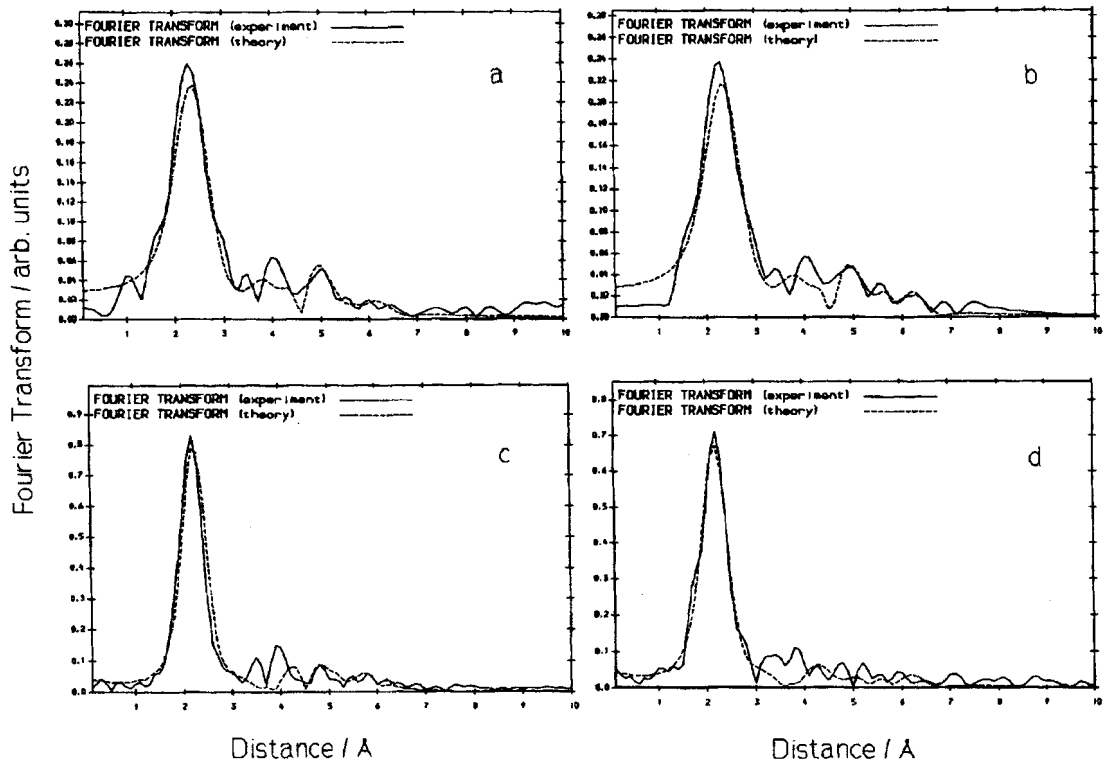

FIGURE 9 EXAFS experimental Fourier Transforms for the Cd [(a) and (b)] and Pb [(c) and (d)] edges in $Cd_{0-4}Pb_{0-6}F_2$ at 300 and 500 K, respectively.

even below room temperature, a phenomenon that is not observed in both pure CdF_2 and PdF_2. The significant reduction in T_c could be ascribed to the very low formation energy of anion Frenkel pairs. These features are consistent with the previous Raman scattering studies conducted on these materials [14] and molecular dynamics investigations on rare-earth doped fluorites [18].

An analysis of MD results of $Cd_{0.4}Pb_{0.6}F_2$ further reveals that no increase in MSD with time of the cations, Cd^{2+} and Pb^{2+}, is observed. Hence, the crystal has not melted in the temperature range of concern since all sublattices do not show an increase in MSD with time. However, the two cations vibrate with very large amplitudes compared with those of pure systems, CdF_2 and PbF_2.

EXAFS plots show that the amplitude of the second peak in the Cd(K) edge Fourier transform of CdF_2 progressively diminishes (compared with that of the first peak) with an increase in temperature. However, for the $Pb(L_{111})$ edge of PbF_2, the second peak diminishes and splits into two. There is presently no obvious explanation for the splitting phenomenon, however it could be related to the more disorder around Pb edges. In addition, the peaks of the Pb^{2+} cations are short in height. Examination of the results given in Tables IV and V shows that the Cd–F radial distances accord well with a value of 2.33 Å obtained for Ca–F in nominally pure CaF_2. Furthermore, the Pb–F bond lengths are longer than those of the Cd–F bond lengths. It must be pointed out that these experimental EXAFS features for the two cations are qualitatively reproduced by our simulation results.

In the case of $Cd_{0.4}Pb_{0.6}F_2$, RDFs derived from computer simulations and EXAFS measurements have a common feature, *i.e.*, they contain only one well-defined peak and their qualitative form is the same. A further feature is that no significant structure is observed in the Fourier transform (Fig. 9) at distances more remote than the first neighbours. This clearly contrasts with the parent materials CdF_2 and PbF_2 which show contributions to the EXAFS from the second neighbours. A possible explanation for the absence of peaks due to cation–cation shells in the doped sample could be the high degree of disorder in the mixed crystal than in the parent materials, CdF_2 and PbF_2.

It can be seen by inspection from Figure 7 (MD results on $Cd_{0.4}Pb_{0.6}F_2$) that the peaks in the Pb–F profiles are broader compared with those from Cd–F radial distances. The results further indicate a significant reduction in the Pb–F amplitudes with temperature increase while those of the Cd–F peaks do not change within the accuracy of the analysis. There is good

agreement with EXAFS results (see Figs. 7 and 9) and minor discrepancies are probable within the errors of the experimental results and the uncertainties in the calculations attributable to the quality of the interionic potentials. The significant broadening of the Pb–F peak with an increase in temperature is attributed to extra F^- vacancies which are present in interstitial sites. These features suggest that the local structural environment of Pb^{2+} ions is more disordered than that of the Cd^{2+} ions. A similar behaviour was noted by Cox *et al.* [7] on $PbSnF_4$. Consequently, more F^- ion vacancies are located around the Pb^{2+} cations in the fluorite structure of $Cd_{0.4}Pb_{0.6}F_2$ than near Cd^{2+} ions.

Values of RDFs obtained from the MD and EXAFS results (Tabs. VI and VII) are comparable. It is also apparent that the Debye-Waller factors obtained in all our analyses are high for the Pb edge, reflecting the extensive disorder around the Pb cations in $Cd_{0.4}Pb_{0.6}F_2$. The findings further show that Cd–F distances in $Cd_{0.4}Pb_{0.6}F_2$ are shorter than those for Pb–F in all cases (see Tabs. VI and VII), which correlates with recent findings by Shimojo *et al.* [19] and Wang *et al.* [21] on $(ZrO_2)_{1-x}(Y_2O_3)_x$, where the host-anion bond lengths are always short. Furthermore, previous observations by Cox *et al.* [7] on compounds such as $RbBiF_4$ (where Rb–F bond length > Bi–F bond length and $rRb^{1+} = 1.47$ Å, $rBi^{3+} = 0.96$ Å) suggested that cations with larger ionic radius such as Pb^{2+} ($rPb^{2+} = 1.20$ Å, $rCd^{2+} = 0.97$ Å) promote vacancy stabilisation in the nearest neighbour shell of the dopant ions. Qualitatively a similar behaviour was observed for the Pb edge in $PbSnF_4$, [3, 7, 8], where Pb–F distance > Sn–F distance. This is also in line with recent findings which strongly correlates the ionic radii with bond lengths in ionic crystals [20]. Hence, in $Cd_{0.4}Pb_{0.6}F_2$ vacancy stabilisation could be expected to occur in the nearest neighbour shell of Pb ions.

The distances (obtained from MD calculations) between the Cd–Cd pairs are shorter than those between the Cd–Pb or Pb–Pb (see Tab. VIII), which means that the tetrahedra formed by four neighbouring cations in the fcc lattice are deformed locally. The shorter Cd–Cd distances are ascribed to the strong Coulomb attraction between Cd ions in corners of a tetrahedron and F^- ion inside the tetrahedron. The MD results further indicate that the Pb–F bond distances reduce with an increase in temperature, while there is hardly any change in Cd–Cd, Pb–Cd, and Pb–Pb distances.

EXAFS studies of $RbBiF_4$ and $PbSnF_4$ [3, 7] suggested that the dopants (Rb and Pb) in these two mixed-metal fluorides play important roles in producing high conductivities that one observed experimentally [14] (1989). Moreover, the dopant cations are envisaged as playing the role of 'interstitial generators', donating F^- ions to interstitial sites. Other cations

(Bi and Sn in $RbBiF_4$ and $PbSnF_4$) play a crucial role in elevating the conductivity by maintaining a temperature-independent local environment, and thus helping to preserve the open-nature of the fluorite structure, retaining the pathway for migration *via* interstitial sites. The same apply to the roles of Cd and Pb ions in $Cd_{0.4}Pb_{0.6}F_2$.

In conclusion, our results suggest that doping $Cd_{1-x}Pb_xF_2$ at 60% PbF_2 increases the disorder around Pb. Furthermore, Kosacki *et al.* [13] also observed that the ionic transport processes in the investigated solid solution ($Cd_{1-x}Pb_xF_2$) are determined by the movement of those fluorine ions whose nearest neighbourhood contains the Pb ions, an idea well supported by our simulations and EXAFS results in the current study. Hence, the overall agreement in our EXAFS and simulation bond lengths is heartening and provides support that the compound $Cd_{0.4}Pb_{0.6}F_2$ can serve as a better electrolyte in future microbatteries due to its high ionic conductivity at relatively low temperatures.

Acknowledgement

The authors wish to thank Prof. C. R. A. Catlow and Dr. G. Sankar of the Royal Institution of Great Britain for their useful discussions. The EXAFS work was made possible by the financial support from the British Overseas Development Agency.

References

[1] Brass, A. M. (1989). "Molecular dynamics study of the defect behaviour in fluorite structure crystals close to the superionic transition", *Phil. Mag. A*, **59**, 843.
[2] Bingham, D., Cormack, A. N. and Catlow, C. R. A. (1989). "A molecular dynamic simulation of gadolinium-doped SrF_2", *J. Phys.*, **1**, 1213.
[3] Catlow, C. R. A., Chadwick, A. V., Greaves, G. N. and Moroney, L. M. (1985). "EXAFS studies of disorder in crystalline ionic solids", *Cryst. Lat. Def. Amorphous Mater.*, **12**, 193.
[4] Catlow, C. R. A. (1986). "Computer simulation studies of transport in solids", *Ann. Rev. Mat. Sci.*, **16**, 517.
[5] Catlow, C. R. A., Cox, P. A., Jackson, R. A., Parker, S. C., Price, G. D., Tomlinson, S. M. and Vetrivel, R. (1989). "Industrial applications of simulation studies in solid state chemistry", *Mol. Simulations*, **3**, 49.
[6] Catlow, C. R. A. (1980). "Structure and transport in superionic fluorites", *Comments Solid State Phys.*, **9**, 157.
[7] Cox, P. A., Catlow, C. R. A. and Chadwick, A. V. (1994). "EXAFS and molecular modelling studies of Rbl-Xbixfl + 2X", *J. Mat. Sci.*, **29**, 2725.
[8] Cox, P. A., Catlow, C. R. A., Chadwick, A. V. and Moroney, L. M., "An EXAFS study of the temperature-induced structural changes in $PbSnF_4$", to be published.
[9] Jacobs, P. W. M., Sahni, V. C. and Vempati, C. S. (1984). "A quasiharmonic calculation of perfect-crystal and instrinsic-defect properties of $\beta-PbF_2$", *Phil. Mag. A*, **49**, 301.

[10] Kosacki, I., Walach, Ya. M. and Litwinczuk, A. P. (1985). "Ionic conductivity and Raman scattering in PbF_2 superionic crystals", *Solid State Commun.*, **53**, 373.
[11] Kosacki, I., Hibner, K., Litwinczuk, A. P. and Valakh, M. Ya. (1986). "Lattice dynamics and ionic conductivity of PbF_2: 6% LiF_2 superionic crystals, *Phys. Status Solidi*", **134**, 495.
[12] Kosacki, I., Hibner, K. and Stefanski, T. (1987). *Acta Phys. Pol. A*, **71**, 409.
[13] Kosacki, I. and Zalibowski, K. (1988). "Polarization phenomena in PbF_2 superionic crystals", *Phys. Stat. Sol.* (*a*), **108**, 765.
[14] Kosacki, I. (1989). "Physical properties and applications of $Cd_{1-x}Pb_xF_2$ superionic crystals", *Appl. Phys. A*, **49**, 413.
[15] Kosacki, I., Litvinchuk, A. P., Tarasov, J. J. and Valakh, M. Ya. (1989). "Anion disordering and specific heat of $Cd_{1-x}Pb_xF_2$ super-ionic crystals", *J. Phys. C*, **1**, 929.
[16] Netshisaulu, T. T., Ngoepe, P. E., Comins, J. D. and Catlow, C. R. A. (1993). "Ion transport studies in cadmium fluoride", *Proc. Int. Conf. Def. Ins. Mater.*, Eds., Spaeth, J. M. and Karnet, O. (World Scientific Publishers), p. 979.
[17] Netshisaulu, T. T. (1996). "Computer simulation and spectroscopic studies of pure and doped cadmium fluoride at high temperature", University of the North, South Africa.
[18] Ngoepe, P. E. and Catlow, C. R. A. (1991). "Molecular dynamics study of ion transport in CaF_2 (10 mol% LaF_3)", *Rad. Eff. and Def. Sol.*, **119**, 399.
[19] Shimojo, F. and Okazaki, H. (1992). "Molecular dynamics studies of yttria stabilized zirconia. I. Structure and oxygen diffusion", *J. Phys. Soc. Jpn.*, **61**, 2848.
[20] Veal, B. W., Mckale, A. G., Paulikas, A. P., Rothman, S. J. and Voronin, B. M. (1995). "Some simple thermodynamic approaches to superionic disorder in fluorite-type crystals: Applications to $SrCl_2$ and K_2S", *J. Phys. Chem. Sol.*, **56**, 839.
[21] Wang, Y. R., Lu, K. Q., Wang, D. H., Wu, Z. H. and Fang, Z. Z. (1994). "EXAFS study of nanocrystalline zirconia", *J. Phys. C*, **6**, 633.